KSCE Journal of Civil Engineering (2022) 26(12):5318-5327
DOI 10.1007/s12205-022-2065-2

pISSN 1226-7988, eISSN 1976-3808
www.springer.com/12205

Tunnel Engineering

Three-Dimensional Upper Bound Limit Analysis of Tunnel Stability with an Extended Collapse Mechanism

Zhizhen Liu[a], **Ping Cao**[a], **Fei Wang**[b], **Jingjing Meng**[c], **Rihong Cao**[a], **and Jingshuo Liu**[d]

[a]*School of Resource and Safety Engineering, Central South University, Changsha 410083, China*
[b]*Yellow River Laboratory, School of Hydraulic Science and Engineering, Zhengzhou University, Zhengzhou 450001, China*
[c]*Dept. of Civil, Environmental and Natural Resources Engineering, Luleå University of Technology, Luleå 97187, Sweden*
[d]*Dept. of Hydraulic Engineering, Hunan Polytechnic of Water Resources and Electric Power, Changsha 410131, China*

ARTICLE HISTORY

Received 23 November 2021
Revised 11 June 2022
Accepted 17 July 2022
Published Online 27 September 2022

KEYWORDS

Three-dimensional collapse mechanism
Tunnel stability
Nonlinear Mohr-Coulomb failure criterion
Upper bound limit analysis
Support pressure
Collapse range prediction

ABSTRACT

A three-dimensional collapse mechanism that can consider a combined collapse of the tunnel roof and the side walls is proposed in this work. The three-dimensional upper bound support pressure is formulated with the power balance principal in the upper bound theorem. The nonlinear Mohr-Coulomb failure criterion is used to replace the commonly used linear Mohr-Coulomb failure criterion. The method has been validated by a series of examples, in which the three-dimensional collapse mechanism and support pressures are in a good agreement with the numerical results and solutions found in the literatures. Furthermore, sensitivity analyses of the geotechnical and geometrical parameters on the support pressure are conducted and the collapsing range is measured. The results show that a higher value of nonlinear failure coefficient, tensile strength, initial cohesion and tangential internal friction angle can increase tunnel stability, while tunnel stability is threatened by a higher value of burial depth, unit weight, tunnel width and height. The predicted collapse range increases noticeably with the increase of the nonlinear coefficient. This study is of great significance for predicting the three-dimensional safety support pressure and collapse mechanism of tunnel.

1. Introduction

There is a trade-off between reinforcement measures and economical costs for the tunneling industry. To avoid overly conservative or unsafe tunnel design, it is necessary to calculate the sufficient support pressure for a tunnel. Thus, an accuracy calculation method that can assess the tunnel stability and predict collapse ranges is vital. The three-dimensional (3D) tunnel stability analysis is of particular interest in this work.

Upper bound limit analysis is one of the most popular methods to the tunnel stability analysis due to its rigorous theoretical basis and wide usage (Senent et al., 2020; Zhang and Zhang, 2020). It has been widely adopted to estimate the limit support pressure for tunnels (Zou et al., 2019; Liu et al., 2020). The research results show that the assumed collapse mechanism in limit analysis plays a critical role in the calculation process (Zhang et al., 2015). Thus, various collapse mechanisms have been proposed for tunnel stability analysis. Davis et al. (1980) introduced four classic two-dimensional (2D) collapse mechanisms of circular tunnel, as shown in Figs. 1(a) – 1(d), while Lyamin et al. (2001) proposed four 2D collapse mechanisms of square tunnel, as shown in Figs. 1(e) – 1(h). Based on these collapse mechanisms, Assadi and Sloan (1991) and Osman et al. (2006) have investigated the limit collapse load of tunnels under the undrained condition. To consider the random collapse characteristics of geotechnical materials, Fraldi and Guarracino (2010) proposed a curved kinematically admissible collapse mechanism. Afterwards, Lyu et al. (2020) further study the stability of deep tunnel based on the method of Fraldi and Guarracino (2010). Besides, a loose zone collapse mechanism (Wang et al., 2014), and a single and multiple blocks collapse mechanism (Wilson et al., 2017), have been proposed and more factors have been considered in these new collapse mechanisms.

Although the significant progress has been made regarding

CORRESPONDENCE Jingjing Meng jingjing.meng@ltu.se Dept. of Civil, Environmental and Natural Resources Engineering, Luleå University of Technology, Luleå 97187, Sweden

© 2022 Korean Society of Civil Engineers

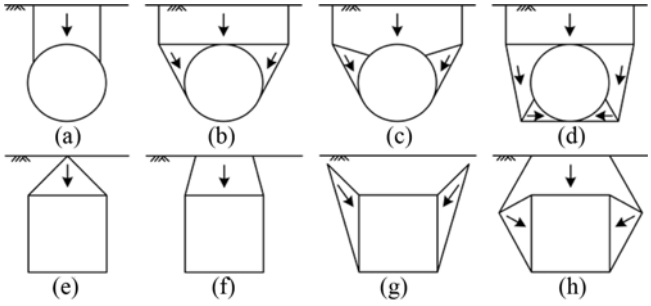

Fig. 1. The Collapse Mechanisms for Tunnels. Four Collapse Mechanisms for a Circular Tunnel (Davis et al., 1980): (a) Roof Collapse, (b) Roof-Sides Collapse, (c) Combination of Roof and Roof-Sides Collapse, (d) Roof, Side Walls and bottom Collapse. Four Collapse Mechanisms for a Square Tunnel (Lyamin et al., 2001)), (e) Local Roof Collapse, (f) Global Roof Collapse, (g) Local Wall Collapse, (h) Local or Global Roof and Wall Collapse

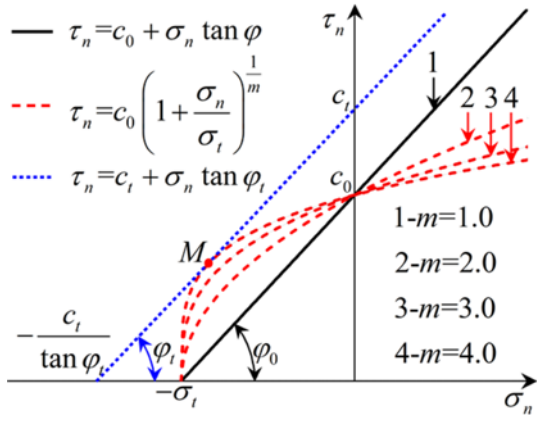

Fig. 2. The Linear and Nonlinear Criterion and the Generalized Tangential Technique

tunnel stability analyses with 2D limit analysis, the inherent errors are inevitably found in its results when applying to 3D tunnel stability (Guan et al., 2017). Accordingly, numerous studies have been performed to extend the method to 3D tunnel stability, and various 3D collapse mechanisms have been proposed such as a 3D rotational collapse mechanism (Huang et al., 2013), a 3D collapse mechanism for shallow cavity with arbitrary profile (Luo and Yang, 2018), a 3D cylinder collapse mechanism (Augarde et al., 2003), an approximate cylinder collapse mechanism (Wang et al., 2019) and a 3D progressive collapse mechanism (Qin and Chian, 2018). Most recently, Park and Michalowski (2020) proposed a 3D roof collapse mechanism that consists of two parts: one part is a right elliptical cone with a piece-wise linear generatrix, and another a prismatic section inserted between the two halves of the cone. As far as authors know, the available 3D collapse mechanisms are restricted to the collapse of tunnel roof. Few studies have conducted on the collapse of tunnel side walls to the stability of tunnels. However, the collapse of side walls is often involved in tunnel collapse accidents, although roof collapse is a major concern in current tunneling industry.

This study aims to develop a 3D collapse mechanism that can consider the combined collapse of both tunnel roof and side walls. The 3D upper bound limit analysis is formulated with the proposed collapse mechanism and the nonlinear Mohr-Coulomb failure criterion. A series of tunnel stability problems have been studied with the proposed approach. Numerical results regarding support pressure and collapse range are in a good agreement with numerical results and solutions found in the literature. Furthermore, sensitivity analysis has been performed to investigate the impact of the geotechnical and geometrical parameters on the upper bound support pressure and collapse range. The presented charts on the support pressure can assist practical engineers to estimate tunnels' stability.

2. 3D Upper Bound Limit Analysis of Tunnels

2.1 Nonlinear Mohr-Coulomb Failure Criterion

The nonlinear criterion not only has the advantage of simple expression, but also its parameters have explicit physical meanings (Yu et al., 2019). Therefore, it is widely used to predict and assess the safety and stability of tunnel, slope and foundation, etc. The nonlinear criterion is given as:

$$\tau_n=c_0\left(1+\frac{\sigma_n}{\sigma_t}\right)^{\frac{1}{m}} \tag{1}$$

where τ_n represents the shear stress in the plastic yield state; σ_n represents the normal stress in the plastic yield state; c_0 stands for the initial cohesion; σ_t represents the tensile stress; and m represents a nonlinear parameter that no less than 1. When m is equal to 1, the nonlinear criterion is transformed into classic linear Mohr-Coulomb failure criterion:

$$\begin{cases}\tau_n=c_0+\sigma_n\tan\varphi_0\\ \tan\varphi_0=\dfrac{c_0}{\sigma_t}\end{cases} \tag{2}$$

where φ_0 represents the initial internal friction angle.

In Fig. 2, the red dash curves are used to indicate nonlinear criterion with the different nonlinear parameters m. The linear Mohr-Coulomb failure criterion is shown with a black line. The straightforward implementation of the nonlinear criterion in the limit analysis is difficult. Fortunately, a generalized tangential technique was proposed with the help of tangential method (Yang and Yin, 2004). The generalized tangential technique is a method which can simplify the nonlinear criterion curve to a series of lines. As shown in Fig. 2, at a certain stress sate indicated by the point M, the nonlinear shear strength is treated as the tangent line on the curve, i.e., blue dot line in Fig. 2. The tangent is given as:

$$\begin{cases}\tau_n=c_t+\sigma_n\tan\varphi_t\\ \tan\varphi_t=\dfrac{d\tau_n}{d\sigma_n}\end{cases} \tag{3}$$

where φ_t represents the tangential internal frictional angle, c_t stands for the tangential cohesion, as shown in Fig. 2. Thus,

substituting Eq. (3) in Eq. (1), the nonlinear criterion may be reformulated as:

$$\begin{cases} \tan\varphi_t = \dfrac{d\tau_n}{d\sigma_n} = \dfrac{c_0}{m\sigma_t}\left(1+\dfrac{\sigma_n}{\sigma_t}\right)^{\frac{1-m}{m}} \\ c_t = \dfrac{m-1}{m}c_0\left(\dfrac{m\sigma_t\tan\varphi_t}{c_0}\right)^{\frac{1}{1-m}} + \sigma_t\tan\varphi_t \end{cases} \tag{4}$$

2.2 3D Collapse Mechanism

The extended 3D collapse mechanism for rectangle tunnels that can consider the both collapse of the tunnel roof and side walls is proposed. Its sketch and associated kinematically admissible velocity field are shown in Fig. 3. In Fig. 3, H, h and w are the tunnel burial depth, height and width, respectively. D is the diameter of the collapse block B_1. The uniform support pressure acting on the tunnel roof and two side walls are represented by q and e, respectively. It is assumed that that $e = Kq$, where K stands for the lateral pressure coefficient. Its cross-sectional view in xoz plane is shown in Fig. 3(a).

Regarding the velocity field as shown in Fig. 3(c), v_0 represents the absolute slide velocity for the collapse block B_1, v_1 indicates the absolute slide velocity for the collapse blocks B_2 tending to slide into the tunnel and the relative slide velocity is indicated with v_{01}.

Since the associate flow rule is used in this study, the angle between the velocity v_1 and the velocity discontinuity boundary S_1 is equal to the angle between the relative velocity v_{01} and the velocity discontinuity boundary S_2. According to the upper bound limit analysis theorem, the absolute velocities v_0, v_1 and relative velocity v_{01} meet the triangle law of vector in the kinematically

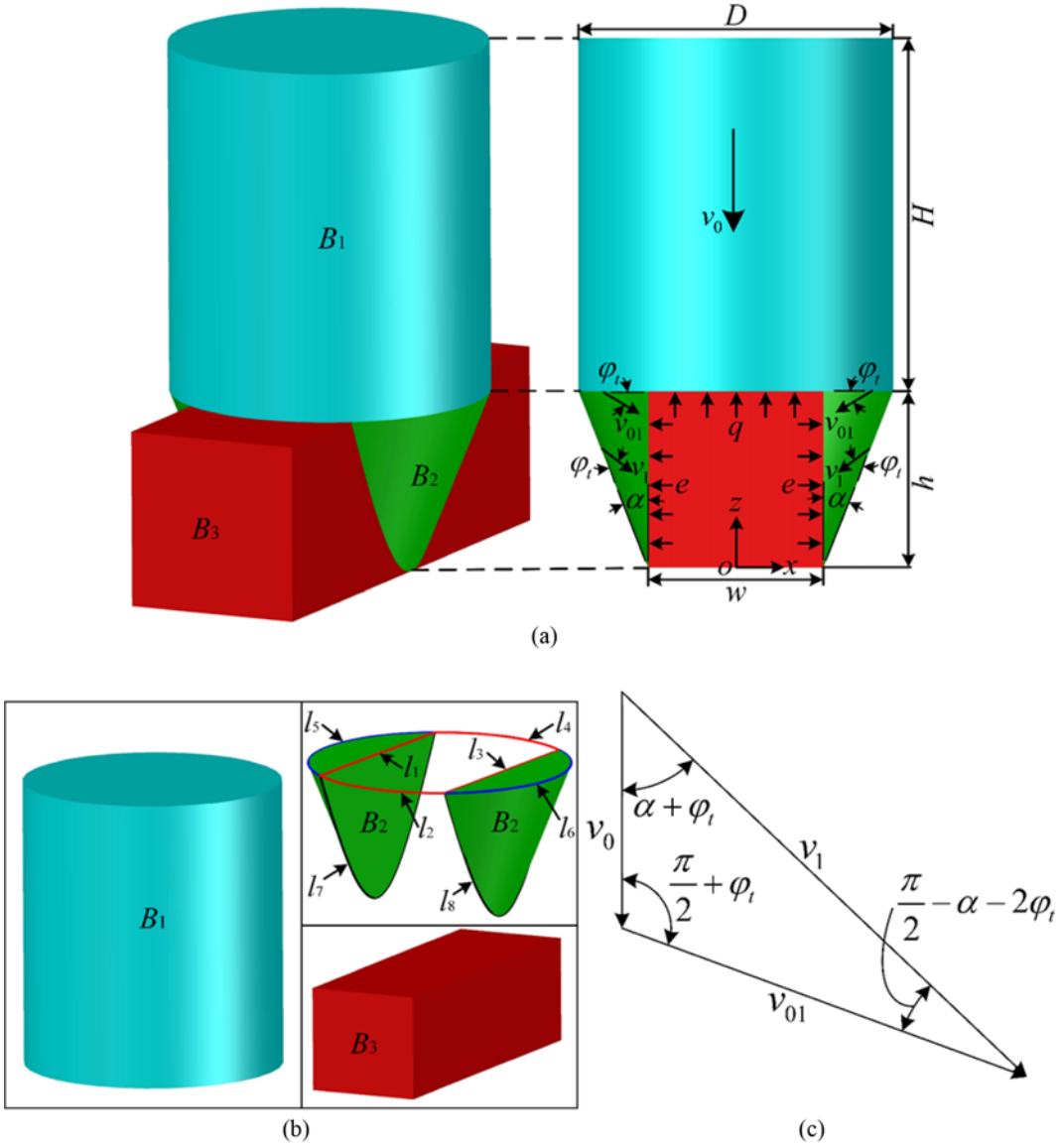

Fig. 3. The 3D Extended Collapse Mechanism and Its Velocity Field: (a) The 3D Collapse Mechanism and Its Sectional View, (b) Three Elements of the Collapse Mechanism, (c) kInematically Admissible Velocity Field

admissible velocity field, as shown in Fig. 3(c), which can be formulated as:

$$\begin{cases} v_1 = \dfrac{\cos\varphi_t}{\cos(\alpha+2\varphi_t)}v_0 \\ v_{01} = \dfrac{\sin(\alpha+\varphi_t)}{\cos(\alpha+2\varphi_t)}v_0 \end{cases} \tag{5}$$

where α represents the collapse angle between the side walls and the velocity discontinuity boundary S_1 and φ_t stands for the tangential internal friction angle.

2.3 Upper Bound Limit Analysis

The key principle for the upper bound limit analysis is that the power of work by external forces is no more than the energy dissipation power in the system (Vo-Minh et al., 2021). Therefore, the power of external forces of this study is caused by the gravity of collapse blocks (B_1 and B_2) and the support pressure q. The power of internal energy dissipation occurs on the two velocity discontinuity surfaces: S_1 and S_2.

2.3.1 The Power of External Forces

The power of gravity for the collapse blocks B_1 and B_2 is:

$$\begin{cases} W_{B_1} = \gamma v_0 y_1 \\ W_{B_2} = \gamma v_0 y_2 \end{cases} \tag{6}$$

where γ is unit weight, and

$$\begin{cases} y_1 = \dfrac{\pi}{4}D^2 H \\ y_2 = \dfrac{\cos\varphi_t\cos(\alpha+\varphi_t)}{\cos(\alpha+2\varphi_t)}\left[y_{21}(h+w\cot\alpha) - \dfrac{2}{3}y_{22}\cot\alpha\right] \end{cases} \tag{7}$$

where the diameter D of the collapse block B_1 is:

$$D = w + 2h\tan\alpha \tag{8}$$

and

$$\begin{cases} y_{21} = \dfrac{1}{2}\left(\dfrac{\pi D^2}{2} - w\sqrt{D^2-w^2} - D^2\arcsin\dfrac{w}{D}\right) \\ y_{22} = \dfrac{D^3}{8}\left[\left(\pi - \arcsin\dfrac{w}{D}\right) - \dfrac{w\sqrt{D^2-w^2}}{D^2} - \left(\dfrac{w}{D}\right)^3 \ln\left(\dfrac{D+\sqrt{D^2-w^2}}{w}\right)\right] \end{cases} \tag{9}$$

The power of support pressure q and e is:

$$\begin{cases} W_q = -qv_0 y_3 \\ W_e = -ev_0 y_4 \end{cases} \tag{10}$$

where

$$\begin{cases} y_3 = S_q \\ y_4 = \dfrac{\sin(\alpha+\varphi_t)\cos\varphi_t}{\cos(\alpha+2\varphi_t)}S_e \end{cases} \tag{11}$$

The surface area that the support pressure i.e., q and e, is acting on the S_q and S_e, respectively:

$$\begin{cases} S_q = \dfrac{w\sqrt{D^2-w^2}}{2} + \dfrac{D^2}{2}\arcsin\dfrac{w}{D} \\ S_e = \dfrac{\sqrt{D^2-w^2}}{2}\left[4h + (2w-D)\cot\alpha\right] - \dfrac{w^2\cot\alpha}{2}\ln\left(\dfrac{D+\sqrt{D^2-w^2}}{w}\right) \end{cases} \tag{12}$$

To sum up, the total power of external forces is

$$W_{ext} = W_{B_1} + W_{B_2} + W_q + W_e = v_0\left[\gamma(y_1+y_2) - q(y_3+Ky_4)\right] \tag{13}$$

2.3.2 The Power of Internal Energy Dissipation

The power of internal energy dissipation can be expressed as following:

$$\begin{cases} W_{S_1} = c_t v_0 y_5 \\ W_{S_2} = c_t v_0 y_6 \end{cases} \tag{14}$$

where

$$\begin{cases} y_5 = S_1\dfrac{\cos^2\varphi_t}{\cos(\alpha+2\varphi_t)} \\ y_6 = S_2\dfrac{\sin(\alpha+\varphi_t)\cos\varphi_t}{\cos(\alpha+2\varphi_t)} \end{cases} \tag{15}$$

The area of the velocity discontinuity surface, S_1 and S_2 is

$$\begin{cases} S_1 = \dfrac{\sqrt{1+\cot^2\alpha}}{2}\left[\dfrac{\pi D^2}{2} - w\sqrt{D^2-w^2} - D^2\arcsin\dfrac{w}{D}\right] \\ S_2 = \dfrac{D^2}{4}\left(\pi - 2\arcsin\dfrac{w}{D}\right) - \dfrac{w\sqrt{D^2-w^2}}{2} \end{cases} \tag{16}$$

The total power of internal energy dissipation can be calculated as:

$$W_{int} = W_{S_1} + W_{S_2} = c_t v_0(y_5+y_6) \tag{17}$$

2.3.3 Upper Bound Support Pressure

Based on the core of the upper bound limit analysis, make the external forces' power (i.e., Eq. (13)) equals to the internal energy dissipation's power (i.e., Eq. (17)), the upper bound support pressure can be derived:

$$q = \frac{\gamma(y_1+y_2) - c_t(y_5+y_6)}{y_3 + Ky_4} \tag{18}$$

The extended tunnel 3D collapse mechanism is constrained by the geometric constraint condition of Fig. 3(c), and the expression of geometric constraint for the extended 3D collapse mechanism as following:

$$\begin{cases} \alpha+\varphi_t > 0 \\ \pi/2 - \alpha - 2\varphi_t > 0 \end{cases} \tag{19}$$

The upper bound support pressure for the surrounding rock stability can be obtained by minimizing the objective function

(18), in which the optimization variables are α and φ_t. The constraint to the optimization problem is given in Eq. (19) as demonstrated with the kinematically admissible velocity field in Fig. 3(c). In addition, the critical collapse range can be identified by the collapse angle α from numerical solutions.

3. Numerical Validations

3.1 Deterministic Results for a Rectangle Tunnel

In this study, given the fact that it is hardly found analytical solutions for rectangular tunnel stability problems, the numerical results from the commercial software FLAC3D are treated as numerical benchmark solutions for validation purpose as it is widely used in tunnel engineering practice and its numerical results are well accepted. To validate the proposed approach, a numerical example as shown in Fig. 4 is used. A series of numerical tests with the varied lateral pressure coefficient K = 1.0, 1.1, 1.2, 1.3, 1.4 and 1.5 have been performed.

As shown in Fig. 4, the dimension of the numerical model is 70 m × 70 m × 50 m ($x \times y \times z$). The top surface of the model is free, the four vertical surfaces have roller boundaries, and the bottom surface of the model is fixed. The model is large enough to avoid the influence of the boundary on the deformation and collapse mechanism. The Mohr-Coulomb model is employed to represent the soil. The initial weight stress was balanced before excavation and the full-face excavation is performed in the simulation. The mechanical parameters in (Wang et al., 2014) are used: unit weight γ is 20 kN/m^3, the tangential internal friction angle φ_t is 18°, the initial cohesion c_0 is 10 kPa, the tensile strength σ_t is 30 kPa, the elastic modulus E is 20 GPa and the Poisson's ratio μ is 0.3. The numerical results on the 3D collapse range are shown in Fig. 5. The good agreement between Fig. 3 and numerical results in Fig. 5 indicates that the proposed 3D collapse mechanism and associated velocity field are reasonable.

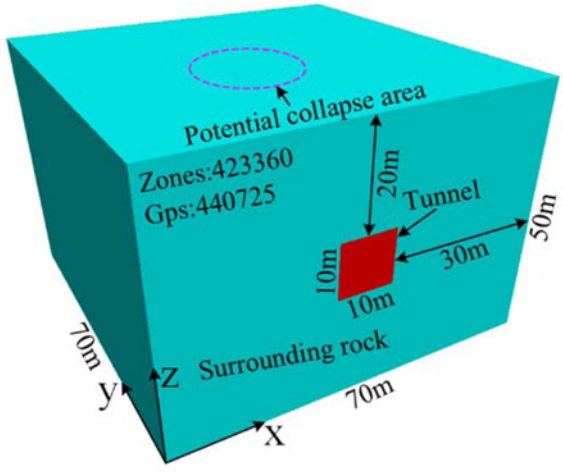

Fig. 4. The Numerical Model of the Rectangle Tunnel

The support pressure obtained by the proposed approach and corresponding relative errors to the results by FLAC3D are listed in Table 1. For comparison, the upper bound limit analysis methods with the mere tunnel roof collapse mechanism (Lyamin et al.,

Table 1. Numerical Result of Support Pressure

q (kPa)	Lyamin et al. (2001)	Wang et al. (2014)	Wang et al. (2019)	This study
K = 1.0	267.0	297.9	335.3	400.9
Re (%)	-29.5	-21.4	-11.5	5.8
K = 1.1	253.1	290.8	--	364.9
Re (%)	-27.5	-16.7	--	4.6
K = 1.2	240.8	283.9	--	336.0
Re (%)	-25.8	-12.6	--	3.5
K = 1.3	230.0	277.3	--	312.2
Re (%)	-24.2	-8.6	--	2.9
K = 1.4	220.4	270.9	--	292.2
Re (%)	-22.9	-5.3	--	2.2
K = 1.5	211.7	264.7	--	275.1
Re (%)	-21.5	-1.8	--	2.1

Note: Re represents relative error. Results by FLAC3D is treated as benchmark solutions and the support pressure corresponding to K = 1, 1.1, 1.2, 1.3, 1.4 and 1.5 is 378.8 kPa, 349.0 kPa, 324.7 kPa, 303.3 kPa, 285.9 kPa and 269.5 kPa, respectively.

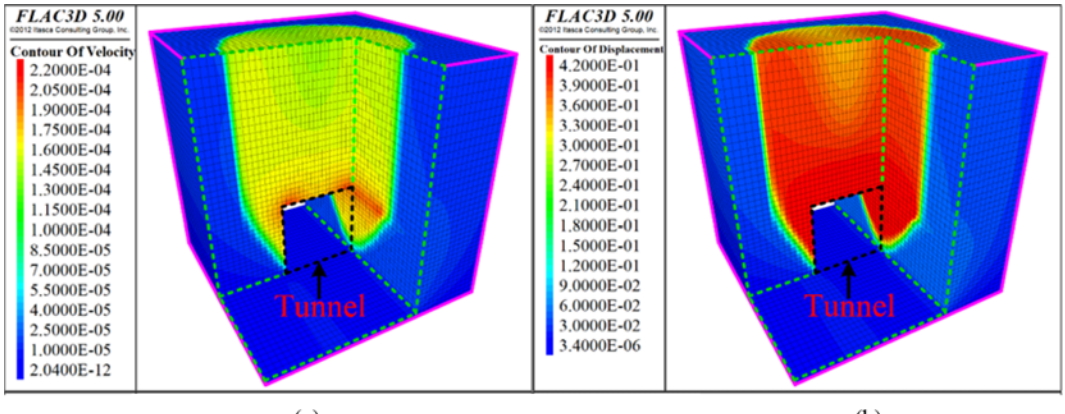

(a) (b)

Fig. 5. 3D Collapse Mechanism: (a) Contour of Velocity, (b) Contour of Displacement

Table 2. Statistical Properties of Random Variables

Random parameters	$E(X)$	$Var(X)$	C_{OV}	ν	σ	Distribution
γ (kN/m^3)	20	5.000	0.25	2.9895	0.1115	Lognormal
φ_t (°)	18	4.500	0.25	2.8835	0.1174	Lognormal
c_0 (kPa)	10	2.500	0.25	2.2902	0.1571	Lognormal
σ_t (kPa)	30	7.500	0.25	3.3970	0.0911	Lognormal
m	1.1	0.275	0.25	-0.0071	0.4525	Lognormal
k	1.1	0.275	0.25	-0.0071	0.4525	Lognormal

2001; Wang et al., 2014; Wang et al., 2019) are used as well. The data shows that upper bound limit methods can predict a very satisfying result. Furthermore, because of the extended collapse mechanism proposed in this work, a smaller relative error is found to the proposed approach than the conventional limit analysis methods for most cases. One exceptional case is found when K is 1.5, in which the relative error for the proposed approach and the limit analysis method (Wang et al., 2014) is 2.1% and -1.8%, respectively. It is necessary to note that comparing to the numerical approach, FLAC3D, the proposed approach is much more efficient: the computation time for FLAC3D and the proposed approach is 1638.1 s and 0.4 s, respectively.

3.2 Stochastic Analysis

The stability of tunnels are highly affected by the geomaterial's spatial variability. A sensitivity analysis toolbox has been developed, which can determine the key input parameters of an output of interest. In this work, stochastic analysis is conducted on the six key mechanical parameters: weight γ, the tangential internal friction angle φ_t, the initial cohesion c_0, the tensile strength σ_t, the nonlinear coefficient and lateral coefficient K. The deterministic value of these parameters as used in Section 3.1 is used as their mean value. Commonly used distribution functions in geomechanics are normal distribution, lognormal distribution and beta distribution (Wu et al., 2019). In order to avoid negative values in geotechnical parameters, the lognormal distribution may be adopted (Li et al., 2021). Therefore, it is assumed that these six parameters follow a lognormal distribution in this study.

The lognormal distribution can be expressed as follows:

$$f(X;v;\sigma)=\frac{1}{X\sigma\sqrt{2\pi}}exp\left[\frac{-(\ln X-v)^2}{2\sigma^2}\right] \tag{21}$$

where v and σ are the mean and standard deviation of the logarithm of the variable, respectively. X is the random variables. The mean ($E(X)$) and variance (V_{ar}) of lognormal distribution meet:

$$E(X)=exp\left(v+\frac{\sigma^2}{2}\right) \tag{22}$$

$$V_{ar}(X)=E(X)\times C_{OV}=exp\left(2v+\sigma^2\right)\left[exp\left(\sigma^2\right)-1\right] \tag{23}$$

where the C_{OV} is the coefficient of variation, a dimensionless coefficient describing the dispersion of each parameter. The range of C_{OV}= 0.25 is a proper value in geotechnical engineering. Then, v and σ are the mean and standard deviation of the logarithm of the variable can be expressed as:

$$v=\log\left[\frac{E(X)^2}{\sqrt{v+E(X)^2}}\right] \tag{24}$$

$$\sigma=\sqrt{\log\left[\frac{v}{E(X)^2+1}\right]} \tag{25}$$

To conduct the stochastic analysis on the random parameters, the Monte Carlo simulation method was used. The probability distribution type of each input parameter is first specified before random sampling is performed from all input parameter sets, and finally a wide range of possible output values is simulated by iterative estimation of randomly sampled samples.In this study, 1000 random samples were generated for each parameter. The random parameters is generated after 1×10^4 iterations of Monte Carlo simulation, as listed in Table 2.

Figure 6 shows distribution of the support pressure under the randomness of different parameters. It is evident that the distribution pattern varies for different random parameters. Deterministic and stochastic results for six random parameters are compared in Fig. 7. The deterministic value is well inside the distribution range.

4. Parameter Analysis

Rock mass type and tunnel geometric parameters have significant influence on tunnel surrounding rock support pressure. Therefore, it is very important to study the support pressure variation of tunnel surrounding rock under different rock mass and geometric parameters. In this section, the geometrical parameters including the tunnel burial depth H, width w and height h and the mechanical parameters including the unit weight γ, the nonlinear coefficient m, the tensile strength σ_t, the initial cohesion c_0, and the tangential internal friction angle φ_t are considered. For simplicity, the lateral coefficient K is set to 1 so the support pressure of the roof q is equal to the support pressure of the side walls e.

4.1 Effect of Burial Depth and Unit Weight

To analyze the sensitivity of the tunnel burial depth H and the unit weight γ on the support pressure, the burial depth H is varied

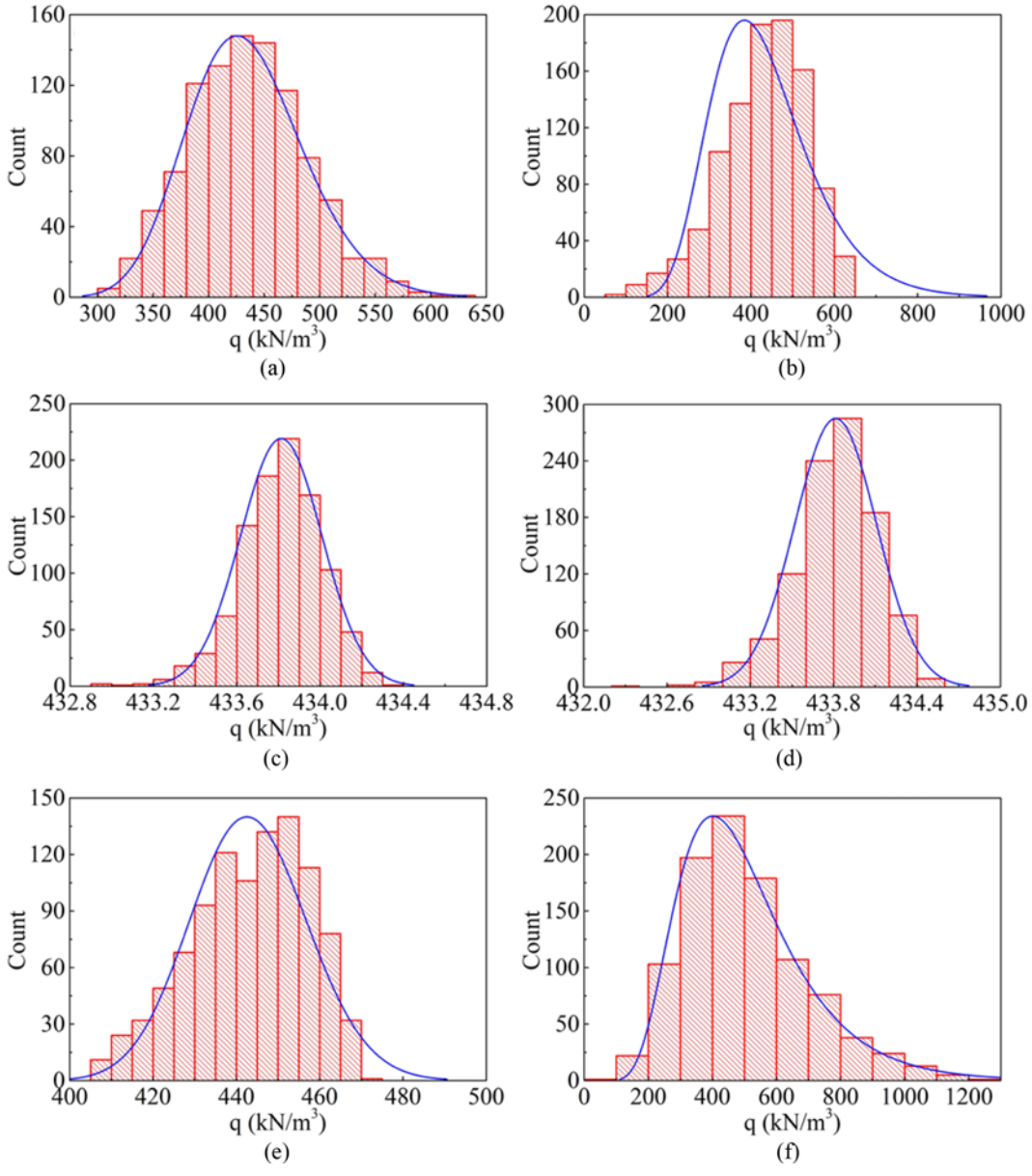

Fig. 6. The Influence of Input Parameters' Random on the Surrounding Rock Support Pressure: (a) The Unit Weight, (b) The Tangential Internal Frictional Angle, (c) The Initial Cohesion, (d) The Tensile Strength, (e) The Nonlinear Coefficient for the Nonlinear Mohr-Coulomb Failure Criterion, (f) The Lateral Pressure Coefficient

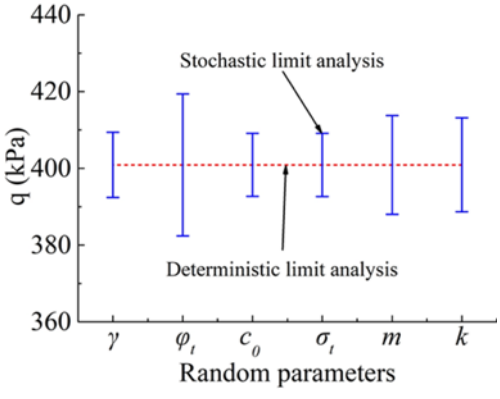

Fig. 7. Deterministic and Stochastic Results foR Six Random Parameters

from 20 m, 25 m, 30 m, 35 m to 40 m; the unit weight γ is varied from 18 kN/m^3, 20 kN/m^3, 22 kN/m^3, 24 kN/m^3 to 26 kN/m^3. The rest parameters remain same as used in the last section. The results can be found in Fig. 8.

It can be observed from Fig. 8 that, the support pressure increases linearly with the increase of the burial depth and the unit weight. It can be found in Fig. 8(a) that, when the burial depth increases from 20 m to 40 m, with the increase of the unit weight from 18 kN/m^3 to 26 kN/m^3, the slope of the increase of the support pressure becomes bigger, which indicates that the support pressure gets more sensitive to the burial depth with the increase of the unit weight. Similarly, when the unit weight increases from 18 kN/m^3 to 26 kN/m^3, with the increase of the

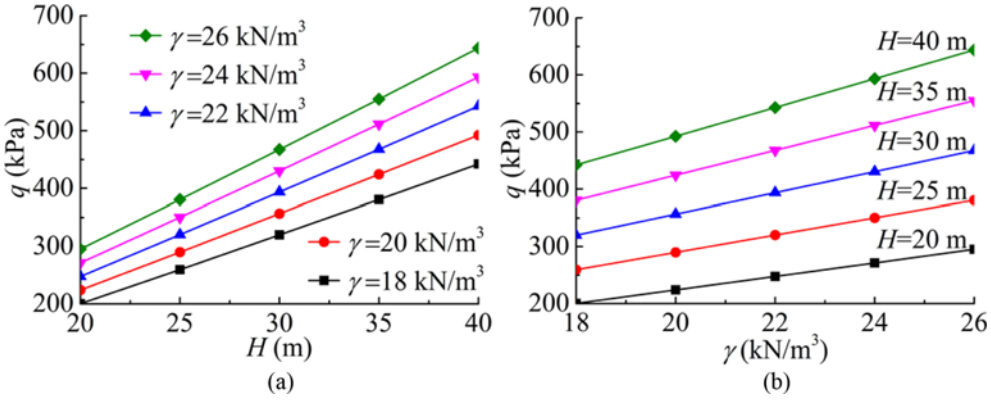

Fig. 8. Effects of Burial Depth and Unit Weight on the support Pressure: (a) Burial Depth of Tunnel H, (b) The Unit Weight γ

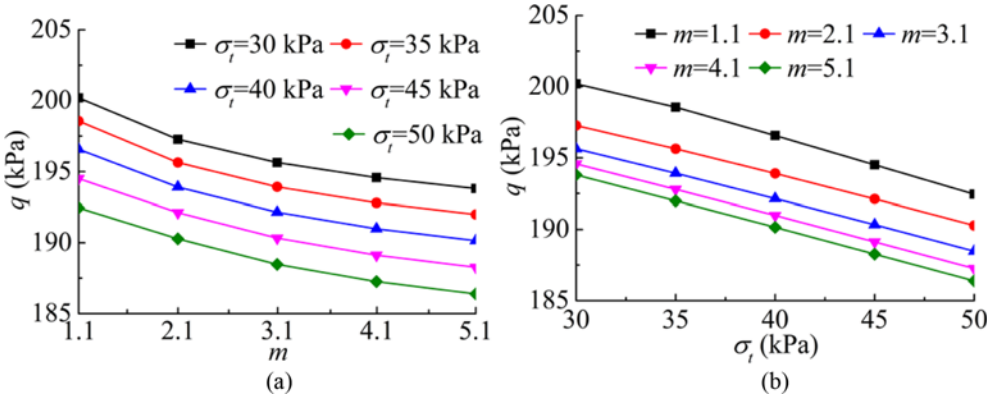

Fig. 9. Effect of Nonlinear Coefficient and Tensile Strength on the Support Pressure: (a) Nonlinear Parameter m, (b) Tensile Strength σ_t

burial depth from 20 m to 40 m, the slope (Fig. 8(b)) of the increase of the support pressure becomes steeper, which implies that the support pressure turns more sensitive to the unit weight with the increase of the burial depth. Moreover, the increase of the support pressure for the case of burial depth is more greatly than that for the case of unit weight, indicating that the support pressure is more sensitive to the burial depth than the unit weight.

4.2 Effect of Nonlinear Coefficient and Tensile Strength

The effect of nonlinear coefficient m and tensile strength σ_t on the support pressure is shown in Fig. 9, in which m is changed from 1.1, 2.1, 3.1, 4.1 to 5.1 and σ_t is ranged from 30 kPa, 35 kPa, 40 kPa, 45 kPa to 50 kPa.

It can be observed from Fig. 9 that, the support pressure decreases obviously with the increase of the nonlinear coefficient and the tensile strength, which implies that the increase the nonlinear parameter and the tensile strength are favorable to the tunnel stability. Furthermore, the influence of the nonlinear coefficient on the support pressure exhibits notably nonlinear feature. The impact of the nonlinear coefficient on the support pressure is more sensitive for a smaller nonlinear coefficient. On the contrary, the decrease rate of the support pressure over the tensile strength is almost constant over the range.

4.3 Effect of Initial Cohesion and Tangential Internal Friction Angle

The effect of initial cohesion c_0 and tangential internal friction angle φ_t on the support pressure is shown in Fig. 10, in which c_0 is changed from 10 kPa, 11 kPa, 12 kPa, 13 kPa to 14 kPa and φ_t is increased from 18°, 20°, 22°, 24° to 26°.

In Fig. 10, the support pressure decreases with the increase of the initial cohesion for a low tangential internal friction angle (i.e., φ_t = 18°). In contrast, there is no significant influence of initial cohesion on the support pressure for relatively high tangential internal friction angles (i.e., φ_t = 20°). Fig. 10(b) indicates that the support pressure decreases with the increase of the tangential internal friction angle. For the cases with a relatively low initial cohesion (i.e., $c_0 \leq 12$ kPa), the decrease rate is nearly constant. The support pressure for the cases with the high initial cohesion (i.e., $c_0 \geq 14$ kPa) and low tangential internal friction angles is significantly lower than that from high initial cohesion cases.

4.4 Effect of Tunnel Width and Height

The effect of tunnel width w and height h on the support pressure is shown in Fig. 11, in which both w and h are varied from 10 m, 12 m, 14 m, 16 m to 18 m.

Figure 11 shows as the tunnel width increases, the support pressure linearly increases overall. Similarly, the support pressure increases with the rise of the tunnel height. In addition, the

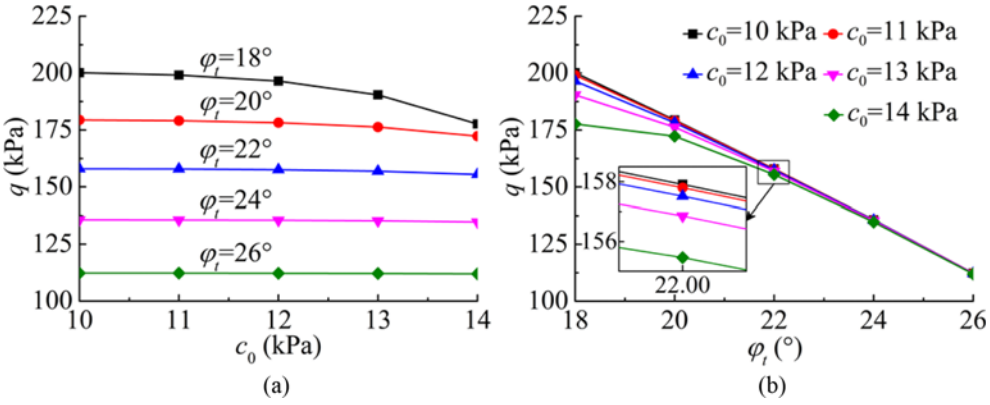

Fig. 10. Effect of Initial Cohesion and Tangential Internal Friction Angle on the Support Pressure: (a) Initial Cohesion c_0, (b) Tangential Internal Friction Angle σ_t

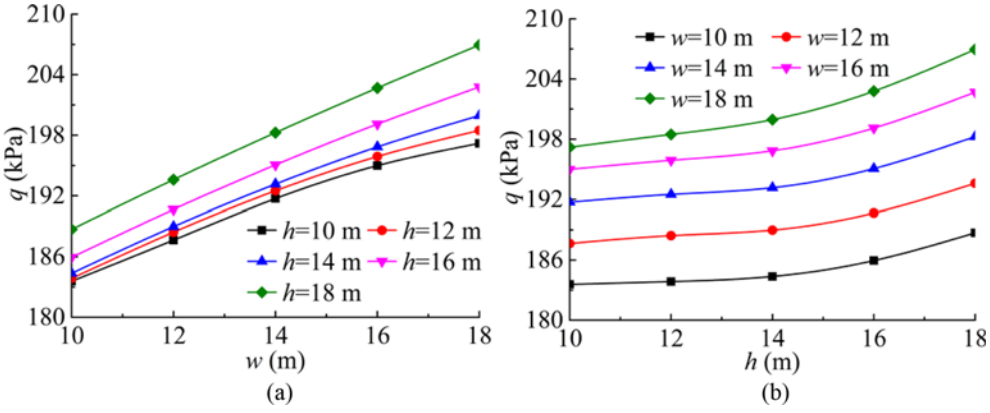

Fig. 11. Effect of Tunnel Width and Height on the Support Pressure: (a) Tunnel Width w, (b) Tunnel Width and Height h

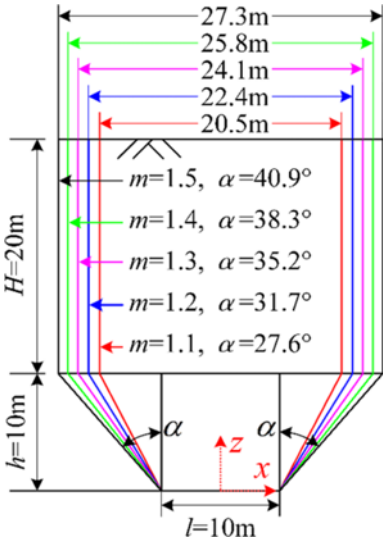

Fig. 12. The Collapse Range with Varied Nonlinear Coefficient

increase rate becomes larger with the increase of tunnel height, indicating the tunnel height is a critical factor for tunnel stability.

4.5 Prediction of Collapse Range

The collapse angle α is obtained from the resolved solution. The results on the predicted collapse range of tunnels with varied nonlinear coefficient m = 1.1, 1.2, 1.3, 1.4 and 1.5 are shown in Fig. 12.

The results show that the collapse range is highly dependent on the nonlinear coefficient. As the nonlinear parameter m varies from 1.1 to 1.5, the collapse diameter rises by 33.2% from 20.5 m to 27.3 m. The reason is that the shear strength is lower for materials with higher nonlinear coefficients at compression.

5. Conclusions

This study proposed an extended 3D collapse mechanism of rectangle tunnels, in which both the collapse of the tunnel's side walls and the roof can be considered. The support pressure and collapse range are derived based on the upper bound limit analysis and the nonlinear criterion. The method is validated through a series of examples, indicating that the extended 3D collapse mechanism can provide a better solution than the conventional upper bound limit analysis. In addition, the sensitivity analysis of various parameters on the support pressure is conducted and collapse range of tunnels is identified.

Acknowledgments

This study was financially supported by the National Natural

Science Foundation of China (5210041777), the Water Conservancy Science and Technology Major Project of Hunan Province (XSKJ2019081-10), the Hunan Province Natural Science Foundation of China (2018JJ0540), the Fundamental Research Funds for the Central Universities of Central South University (2021zzts0281), the CRSRI Open Research Program (SN: CKWV2017512/KY).

ORCID

Zhizhen Liu https://orcid.org/0000-0003-1667-7369
Ping Cao https://orcid.org/0000-0003-3192-0267
Fei Wang https://orcid.org/0000-0003-0482-9644
Jingjing Meng https://orcid.org/0000-0003-0148-9779
Rihong Cao https://orcid.org/0000-0002-6293-6248
Jingshuo Liu https://orcid.org/0000-0002-9156-0120

References

Assadi A, Sloan SW (1991) Undrained stability of shallow square tunnel. *Journal of Geotechnical Engineering* 117(8):1152-1173, DOI: 10.1061/(ASCE)0733-9410(1991)117:8(1152)

Augarde CE, Lyamin AV, Sloan SW (2003) Prediction of undrained sinkhole collapse. *Journal of Geotechnical and Geoenvironmental Engineering* 129(3):197-205, DOI: 10.1061/(ASCE)1090-0241(2003)129:3(197)

Davis EH, Gunn MJ, Mair RJ, Seneviratne HN (1980) The stability of shallow tunnels and underground openings in cohesive material. *Geotechnique* 30(4):397-416, DOI: 10.1680/geot.1980.30.4.397

Fraldi M, Guarracino F (2010) Analytical solutions for collapse mechanisms in tunnels with arbitrary cross sections. *International Journal of Solids and Structures* 47(2):216-223, DOI: 10.1016/j.ijsolstr.2009.09.028

Guan K, Zhu WC, Niu LL, Wang QY (2017) Three-dimensional upper bound limit analysis of supported cavity roof with arbitrary profile in Hoek-Brown rock mass. *Tunnelling and Underground Space Technology* 69:147-154, DOI: 10.1016/j.tust.2017.06.016

Huang F, Yang XL, Ling TH (2013) Prediction of collapsing region above deep spherical cavity roof under axis-symmetrical conditions. *Rock Mechanics and Rock Engineering* 47(4):1511-1516, DOI: 10.1007/s00603-013-0455-y

Li T, Gong, W, Tang H (2021) Three-dimensional stochastic geological modeling for probabilistic stability analysis of a circular tunnel face. *Tunnelling and Underground Space Technology* 118:104190, DOI: 10.1016/j.tust.2021.104190

Liu ZZ, Cao P, Lin H, Meng JJ, Wang YX (2020) Three-dimensional upper bound limit analysis of underground cavities using nonlinear Baker failure criterion. *Transactions of Nonferrous Metals Society of China* 30(7):1916-1927, DOI: 10.1016/s1003-6326(20)65350-x

Luo WJ, Yang XL (2018) 3D stability of shallow cavity roof with arbitrary profile under influence of pore water pressure. *Geomechanics and Engineering* 16(6):569-575, DOI: 10.12989/GAE.2018.16.6.569

Lyamin AV, Jack DL, Sloan SW (2001) Collapse analysis of square tunnels in cohesive–frictional soils. *Computational Mechanics–New Frontiers for the New Millennium* 405-414, DOI: 10.1016/B978-0-08-043981-5.50063-8

Lyu C, Yu L, Wang M, Xia P, Sun Y (2020) Upper bound analysis of collapse failure of deep tunnel under karst cave considering seismic force. *Soil Dynamics and Earthquake Engineering* 132:106003, DOI: 10.1016/j.soildyn.2019.106003

Osman AS, Mair RJ, Bolton MD (2006) On the kinematics of 2D tunnel collapse in undrained clay. *Géotechnique* 56(9):585-595, DOI: 10.1680/geot.2006.56.9.585

Park D, Michalowski RL (2020) Three-dimensional roof collapse analysis in circular tunnels in rock. *International Journal of Rock Mechanics and Mining Sciences* 128:104275, DOI: 10.1016/j.ijrmms.2020.104275

Qin C, Chian SC (2018) Revisiting crown stability of tunnels deeply buried in non-uniform rock surrounds. *Tunnelling and Underground Space Technology* 73:154-161, DOI: 10.1016/j.tust.2017.12.006

Senent S, Yi C, Jimenez R (2020) An upper bound solution for tunnel face stability analysis considering the free span. *Tunnelling and Underground Space Technology* 103:103515, DOI: 10.1016/j.tust.2020.103515

Vo-Minh T, Nguyen-Son L, Nguyen-Van G, Thai-Phuong T (2021) Upper bound limit analysis of circular tunnel in cohesive-frictional soils using isogeometric analysis based on Bézier extraction. *Tunnelling and Underground Space Technology* 114:103995, DOI: 10.1016/j.tust.2021.103995

Wang HT, Liu P, Liu C, Zhang X, Yang Y, Liu LY (2019) Three-dimensional upper bound limit analysis on the collapse of shallow soil tunnels considering roof stratification and pore water pressure. *Mathematical Problems in Engineering* 2019:2019, DOI: 10.1155/2019/8164702

Wang Z, Qiao C, Song C, Xu J (2014) Upper bound limit analysis of support pressures of shallow tunnels in layered jointed rock strata. *Tunnelling and Underground Space Technology* 43:171-183, DOI: 10.1016/j.tust.2014.05.010

Wilson DW, Abbo AJ, Sloan SW, Yamamoto K (2017) Undrained stability of rectangular tunnels where shear strength increases linearly with depth. *Canadian Geotechnical Journal* 54(4):469-480, DOI: 10.1139/cgj-2016-0072

Wu Y, Zhou X, Gao Y, Zhang L, Yang J (2019). Effect of soil variability on bearing capacity accounting for non-stationary characteristics of undrained shear strength. *Computers and Geotechnics* 110:199-210, DOI: 10.1016/j.compgeo.2019.02.003

Yang XL, Yin JH (2004) Slope stability analysis with nonlinear failure criterion[J]. *Journal of Engineering Mechanics* 130(3):267-273, DOI: 10.1061/(ASCE)0733-9399(2004)130:3(267)

Yu L, Lyu C, Wang M, Xu T (2019) Three-dimensional upper bound limit analysis of a deep soil-tunnel subjected to pore pressure based on the nonlinear Mohr-Coulomb criterion. *Computers and Geotechnics* 112:293-301, DOI: 10.1016/j.compgeo.2019.04.025

Zhang C, Han K, Zhang D (2015) Face stability analysis of shallow circular tunnels in cohesive–frictional soils. *Tunnelling and Underground Space Technology* 50:345-357, DOI: 10.1016/j.tust.2015.08.007

Zhang D, Zhang B (2020) Stability analysis of the pressurized 3D tunnel face in anisotropic and nonhomogeneous soils. *International Journal of Geomechanics* 20(4):04020018, DOI: 10.1061/(ASCE)GM.1943-5622.0001635

Zou J, Chen G, Qian Z (2019) Tunnel face stability in cohesion-frictional soils considering the soil arching effect by improved failure models. *Computers and Geotechnics* 106:1-17, DOI: 10.1016/j.compgeo.2018.10.014